Dalton Transactions

Accepted Manuscript

ROYAL SOCIETY OF CHEMISTRY

www.rsc.org/dalton

Iridium-Mediated C–S Bond Activation and Transformation: Organoiridium(III) Thioether, Thiolato, Sulfinato and Thiyl Radical Compounds. Synthesis, Mechanistic, Spectral, Electrochemical and Theoretical Aspects†

Ujjwal Das, Tapas Ghorui, Basab Adhikari, Sima Roy, Shuvam Pramanik and Kausikisankar Pramanik*

Department of Chemistry, Inorganic Chemistry Section, Jadavpur University, Kolkata – 700032, India. E-mail: kpramanik@hotmail.com; Tel: +9133 2457 2781

Abstract

An attractive methodology, single-electron transfer (SET) reductive cleavage of the C–S bond mediated by metal in presence of the external stimuli PPh_3, has been applied to the kinetically inert $IrCl_3$ in order to synthesize thiolato complex $[Ir^{III}(L^{S})Cl(PPh_3)_2]$ **3** from precursor thioether complexes $[Ir^{III}(L^{SR})Cl_2(PPh_3)]$ (R = alkyl) **2**. The aforesaid cleavage process in association with (arene)C–H activation furnishes a new class of organosulfur compounds of iridium(III). The thiolato chelate **3** displays a reversible oxidative wave at 0.75 V *vs* Ag/AgCl signifying its remarkable nucleophilic character. The high electron density on the thiolato-S *vis-à-vis* superior nucleophilicity can be envisaged through the formation of a number of S-centered derivatives. This observation has been accorded with the theoretical scrutiny of HOMO of **3**, which assumes 49% of S_{3p}. Notably, the facile oxidative nature of **3** makes it an apposite precursor for metal-stabilized thiyl radical species. Indeed, iridium(III)-stabilized $\mathbf{3}^{\bullet+}$ can be generated by chemical/electrochemical means. The axial EPR spectra with g ~2.0 along with theoretical analysis of SOMO (S_{3p} 24% + Ph_{π} 43% + d_{yz} 15%) and spin density (ρ_S = +0.543, ρ_{Ph} = +0.315, ρ_{Ir} = +0.151) of one-electron oxidized $\mathbf{3}^{\bullet+}$ validates iridium-stabilized thiyl radical description. This observation suggests that the *CNS* coordination mode in thiophenolato complex **3** is redox-active. Complex **3** is very much prone to S-centered oxidation under normal aerobic condition to yield metallosulfoxide $[Ir^{III}(L^{SO_2})Cl(PPh_3)_2]$ **4**. The enhanced nucleophilicity of thiolato-S can also be manifested *via* the smooth S–C bond making process with alkyl halides (R′X, R′ = Me and allyl; X = Br, I) and subsequent formation of thioether complexes of type $[Ir^{III}(L^{SR'})ClX(PPh_3)]$ **5**. The organosulfur compounds of iridium(III) exhibit rich spectral properties including luminescence and the origin of these transitions are scrutinized with DFT and TD-DFT method.

Introduction

Heavier transition metals including platinum-group-metals mediated C–S bond activation along with the transformation processes are of intriguing interest from the perspective of synthetic, mechanistic, catalytic as well as theoretical chemistry.[1] Notably, the majority of the investigations have been carried out on transition metal compounds in order to understand the C–S bond activation of thiophenes, benzothiophenes, dibenzothiophenes and their derivatives on account of plausible application in hydrodesulfurization (HDS) processes.[2] Recently, noble-metal mediated C–S bond activation and functionalization of the thiolato moiety have been applied in numerous synthetic methods,[3] catalytic reactions,[2b,4] as well as in spectroscopy[5] and biochemistry[6]. In this perspective, new methodology along with detailed mechanistic understanding will be indeed helpful to unveil fundamental insight of C–S bond scission. Moreover, activation of aryl C–H bond in combination with C–hetero atom bond by platinum metals, leads to an easy access of cyclometallated compounds, which are important due to their inherent physicochemical properties.[7] The major understanding of reactivity and mechanism on C–S activation of thiophene and its derivatives have been obtained *via* oxidative addition in a number of Rh(I) and to some extent other low valent noble metals e.g., Pt(0) and Ir(I).[1a,2a,c,d,8] In the recent past, we have reported C(sp^3)–S cleavage of alkyl 2-(phenylazo)phenyl thioether **1** (HL^{SR}; R = Me, CH_2Ph) using Rh(III) by single-electron transfer (SET) mechanism.[9] Reports of iridium-mediated S–C bond activation are less documented in literature and in none of them the reductive cleavage of the carbon–sulfur bond by a SET mechanism is involved.[1a,10] It is worth mentioning that there are only a few reports of reductive cleavage of C–S bond *via* homolytic scission mediated by first transition metals.[11] Hence, our studies on noble-metal interceded C–H and C–S bond activation and transformation have been extended to $IrCl_3$ through the exploration of several organoiridium(III) sulfur compounds *viz*. thioether **2**, thiolato **3**, sulfinato **4** and thioether **5** complexes (Scheme 1).

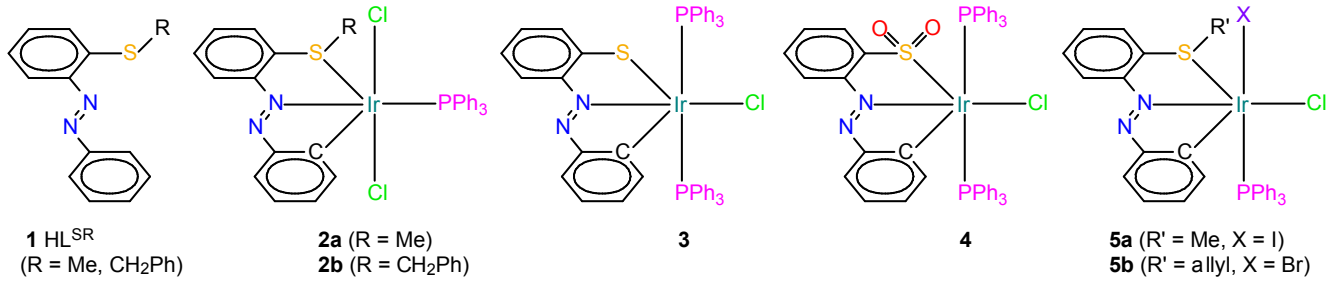

1 HL^{SR} (R = Me, CH_2Ph) **2a** (R = Me) **2b** (R = CH_2Ph) **3** **4** **5a** (R' = Me, X = I) **5b** (R' = allyl, X = Br)

Scheme 1 Ligand and orthometallated iridium(III) sulfur compounds

The organoiridium(III) thiolato compound $[Ir^{III}(L^{S})Cl(PPh_3)_2]$ **3** is formed either *via* both C–S and C–H bond cleavages in **1** in one-pot reaction with $IrCl_3$ or from the corresponding thioether complex $[Ir^{III}(L^{SR})Cl_2(PPh_3)]$ (R = Me, CH_2Ph) **2** in presence of PPh_3. Thiolato **3** is electro-active in solution,

exhibiting facile oxidative response unlike the case of its thioether **2** precursor, indicating high electron density on the thiolato moiety as well as superior nucleophilicity of the non-bridged thiolato-S. This observation leads to the exploration of iridium-bound thiyl radical species $\mathbf{3}^{\bullet+}$. Recently, the stabilization and characterization of metal coordinated thiyl complexes ($M(ArS^{\bullet})L_n$) are of significant interest due to their involvement in various biochemical processes.[12] Till date, work on alkyl and phenylthiyl radicals generated from thiolate ligands have been focused primarily on first-row transition metals.[12c,13] Among noble metals, only a few metal-bound thiyl radicals are reported and they are mainly limited to ruthenium[12a,14] and a few other platinum metals.[9,15]

One of the most noteworthy properties of thiolato functions is their superior nucleophilicity, which leads to derivatives modified at the sulfur center. The sulfur-centered reactivity of transition metal thiolates is reflected in oxygenation[16] and alkylation[17] processes. Molecular oxygen is known to oxidize thiolato ligands to sulfenato or sulfinato and numerous studies of analogous S-centered oxidation of iron, cobalt, nickel and other first row transition metal complexes[16e,18] have been performed as bio mimicking examples[19] of certain sulfur-rich metalloenzymes. Nonetheless, similar scrutiny of thiolato-S oxidation of noble metal complexes are less cited as compared to those of the 3d metals and they are limited mostly to ruthenium, rhodium, palladium, osmium, platinum and gold complexes.[1e,16b,19d,20] To the best of our knowledge there is no report of the analogous studies with iridium. It is worth mentioning that organoiridium(III) thiolato complex **3** is prone to similar type of oxidation under normal aerobic conditions to yield the iridium coordinated metallosulfoxide $[Ir^{III}(L^{SO_2})Cl(PPh_3)_2]$ **4**. The alkylation reactions with alkyl halides have been found exclusively at the sulfur atom of mononuclear **3** to yield neutral thioether complexes of type $[Ir^{III}(L^{SR'})ClX(PPh_3)]$ (R′ = Me, allyl; X = Br, I) **5**.

All the organoiridium(III) sulfur compounds are found to be stable in air as well as in presence of moisture. The geometry of the representative compounds have been authenticated by X-ray diffraction study. Finally, unification and correlation of the observed trends in terms of spectral, electrochemical, structure and bonding are scrutinized with the aid of theoretical study.

Results and Discussion

Syntheses

The reaction of $IrCl_3{\cdot}3H_2O$ and alkyl 2-(phenylazo)phenyl thioether **1** (HL^{SR}; R = Me, CH_2Ph) in the presence of 10-fold excess of PPh_3 in ethanol at reflux gave a mixture of organothioether **2**, organothiolato **3** and organosulfinato **4** in approximately 25, 40, and 10% yield respectively (Scheme 2). The $C(sp^2)$–H bond

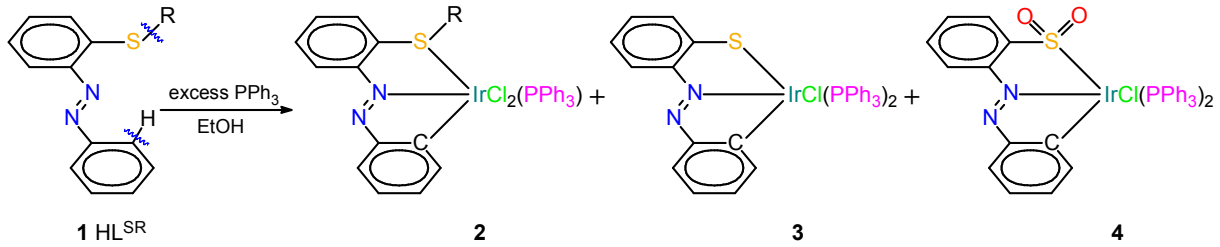

Scheme 2 One-pot synthesis of cyclometallated iridium(III) thioether **2**, thiolato **3** and sulfinato **4** complexes under normal aerobic condition

was cleaved *in situ* prior to the cleavage of the C(sp^3)–S bond and the general accepted mechanism of the formation orthometallation of azobenzene proceeds *via* initial coordination of azo-nitrogen followed by electrophilic substitution at the pendant phenyl ring.[21] It is worth noting that the C–S bond scission was not observed when the reaction was performed with 1 equiv of PPh_3 relative to both **1** and $IrCl_3{\cdot}3H_2O$ and only greenish brown organothioether **2** was obtained in good yield. Significantly, the thioether functionality of **2** is transformed to a thiolato group in the presence of excess PPh_3 to afford **3** *via in situ* C(sp^3)–S bond scission (Scheme 3). Although the S-dealkylation is not observed with $IrCl_3$ in the absence of PPh_3, [$IrCl(PPh_3)_3$] alone is competent of furnishing **3** under analogous conditions in low yield. The organothiolato **3** is found to be highly prone to S-centered oxidation under normal aerobic conditions (atmospheric oxygen) to yield a dark orange metallosulfoxide $Ir^{III}(L^{SO_2})Cl(PPh_3)_2$] **4** in boiling acetonitrile (Scheme 3). The analogous rhodium complex [$Rh^{III}(L^{S})Cl(PPh_3)_2$] did not afford any S-oxygenated species under similar reaction

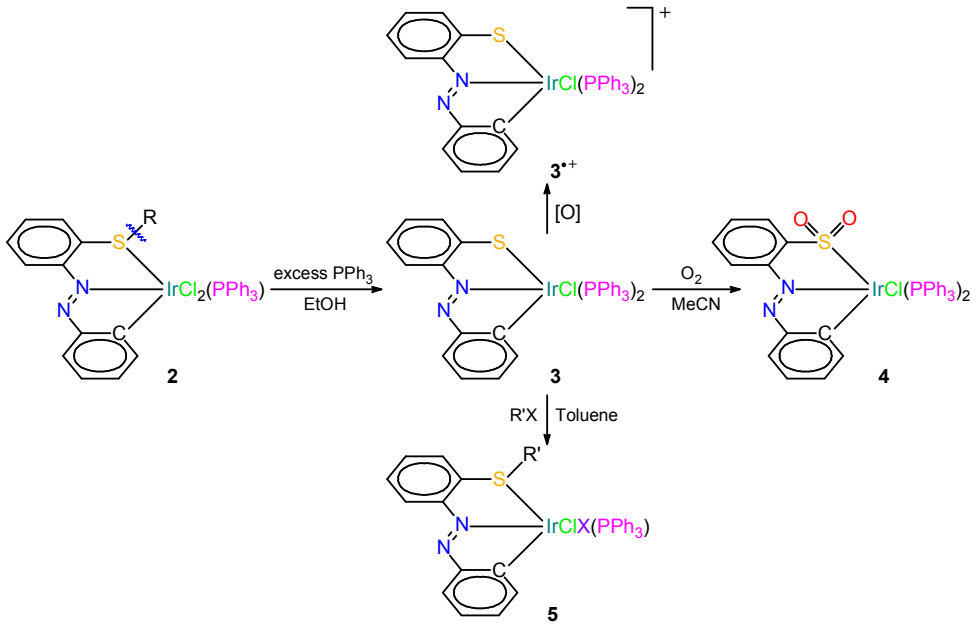

Scheme 3 Conversion of thioether **2** to sulfinato **4** , thioether **5** and thiyl radical **3**$^{\bullet+}$ species *via* thiolato **3**

conditions.[9] Facile S-centered oxidation of **3** relative to the rhodium analogue was reflected in the electrochemical study (*vide supra*). Superior M → S π back-donation in **3** relative to that in the analogous rhodium compound can be accounted to the enhanced S-center reactivity of the former. Better back-donating efficacy of iridium (5d) as compared to that of rhodium (4d) is attributable to the more dilated d orbitals of the former owing to the relativistic effects.[22] It is likely that the formation of sulfinato $\{S(=O)_2\}$ moiety in **4** from **3** proceeds *via* intramolecular and/or intermolecular addition of dioxygen.[20a,f,23] The sulfur-centered reactivity of iridium(III) thiolate was also reflected in its reactivity during alkylation processes. The reaction of **3** with R′X (R′ = Me and allyl; X = Br and I) in refluxing toluene afforded orange organoiridium(III) thioether complexes of type $[Ir^{III}(L^{SR'})ClX(PPh_3)]$ **5** in good yields *via* S–C(sp^3) bond formation. Redox-active thiophenolato coordination in **3** undergoes facile oxidation by chemical/electrochemical means yielding a iridium-bound thiyl radical $\mathbf{3}^{\bullet+}$ in solution (Scheme 3).

C–S Cleavage Mechanism

Two important features are observed in the course of the S–C bond scission mediated by Ir(III). First, the oxidation state of iridium remains the same in both the starting organothioether **2** as well as the organothiolato product **3** and this appears peculiar in the sense that the involvement of metal atom in the cleavage process. Second, the presence of a PPh_3 molecule is necessary during the cleavage process. The latter finding provides a unique opportunity to cleave the C–S bond in a more controlled way since this cleavage reaction does not occur in the absence of PPh_3. Indeed, PPh_3 acts as efficient external stimuli in the cleavage process. Based upon these observations, we propose that an iridium(II) intermediate species must have been formed that could plausibly be involved in the C–S cleavage reaction. However, attempts to detect any iridium(II) intermediates along the reaction pathway were unsuccessful.

A plausible mechanism of the C–S cleavage process is presented in Scheme 4.[9] We anticipate that, after the initial coordination of L^{SR} with metal, the organothioether iridium(III) compounds **2** get reduced in the presence of excess phosphine to the intermediate organothioether iridium(II) complex. In consideration of the anticipated mechanism illustrated in Scheme 4, it is logical to conclude that the conversion of **2** to **3** proceeds through the intermediacy of the Ir(II) species $[Ir(L^{SR})Cl(PPh_3)_2]$ (electron-rich d^7 system), which is

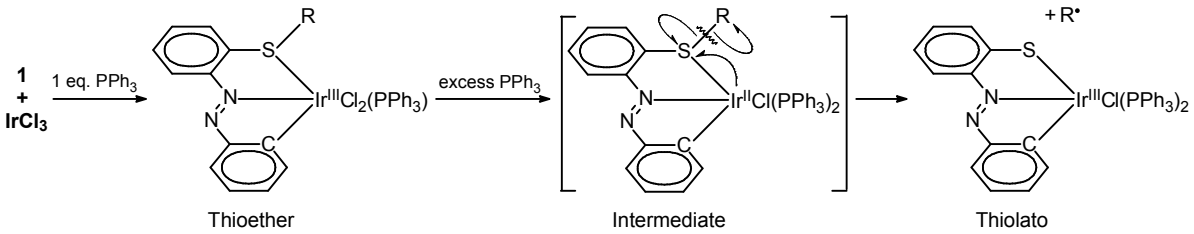

Scheme 4 Proposed mechanism of C–S cleavage

active toward the one-electron reduction of the coordinated S–C(sp^3) bond of thioether group from L^{SR} (*via* electron donation into the C–S σ* antibonding orbital).[1e,24] This results in reductive cleavage of the pendant S–C(alkyl) bond with concurrent extrusion of an alkyl radical ($R^{\bullet}$). Indeed, open debates linger about the preferred pathway for C–S bond cleavage among the three possibilities as shown in Scheme 5. Notably, the anticipated products derived from the cleaved alkyl group vary appreciably with the nature of cleavage process.[25] To ascertain the underlying mechanistic process, a selected ion monitoring GC-MS experiment has been performed with the reaction mixture using benzyl derivative of **1**, HL^{SCH_2Ph}. The cleaved alkyl group is

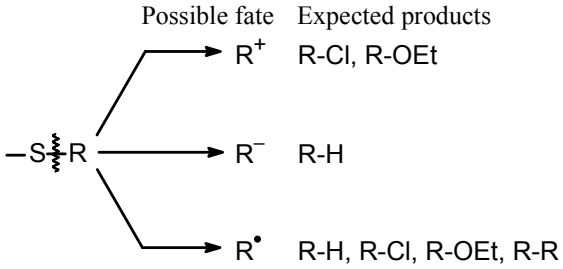

Scheme 5 Possible routes of C–S bond cleavage

transformed to a range of products and the structure-specific signals in the chromatogram are identified as R–H, R–Cl, R–OEt and R–R (Fig. S1, ESI†). The chromatogram is consistent with the reductive cleavage by the single-electron transfer (SET) mechanism since the products (comparable yield of toluene and ethyl benzyl with little benzyl chloride and dibenzyl) appear to be derived from radical species. Since the observed products obtained from the cleaved alkyl group are best matched with the third possibility (Scheme 5), we propose that the cleavage *via* radical pathway is most likely to be operative.[26] The reductive cleavage of the C(sp^3)–S bond of coordinated thioether moiety has been explored as an attractive route to functional ligands and new materials.

Description of the Crystal Structures

The X-ray crystal structures of **2a, 3, 4** and **5b** were determined to explore the geometries about the metal ions and three different bonding modes ($[L^{SR}]^-$, $[L^{S}]^{2-}$ and $[L^{SO_2}]^{2-}$) of the tridentate C^N^S ligand were ascertained. In the all organosulfur compounds, the ligands are orthometallated and coordinate to iridium(III) *via* the *ortho*-carbon C(1), azo-nitrogen N(1), and thiolato sulfur S(1) so as to form two contiguous five-membered chelates. It is to be noted that the iridium(III) cyclometallates with azo function are sparse.[27] Suitable single crystals for X-ray analysis of the respective complex were grown by slow diffusion of hexane

into dichloromethane solution at room temperature. Experimental crystallographic data are summarized in Table S1† in the ESI. Selected metrical parameters are listed in Table 1.

2a. Fig. 1 shows the molecular view and atom numbering scheme of a thioether complex **2a** (R = CH_2Ph). Crystallographic analysis of the thioether complex reveals a distorted octahedral structure with meridional C^N^S coordination and the ligand, $[L^{SCH_2Ph}]^-$, acts as a tridentate monoanionic donor. The coordination sphere of the metal atom is completed by one triphenylphosphine and two *trans* chloride atoms. Expectedly, S1−C12 length is shorter than S1−C13 length (1.783(5) and 1.848(5) Å, respectively, $C(sp^2)$ *vs* $C(sp^3)$). Both S1−C12 and S1−C13 bond lengths of the complex are longer by ca. 0.023 and 0.031 Å as compared to those of the free ligand.[9]

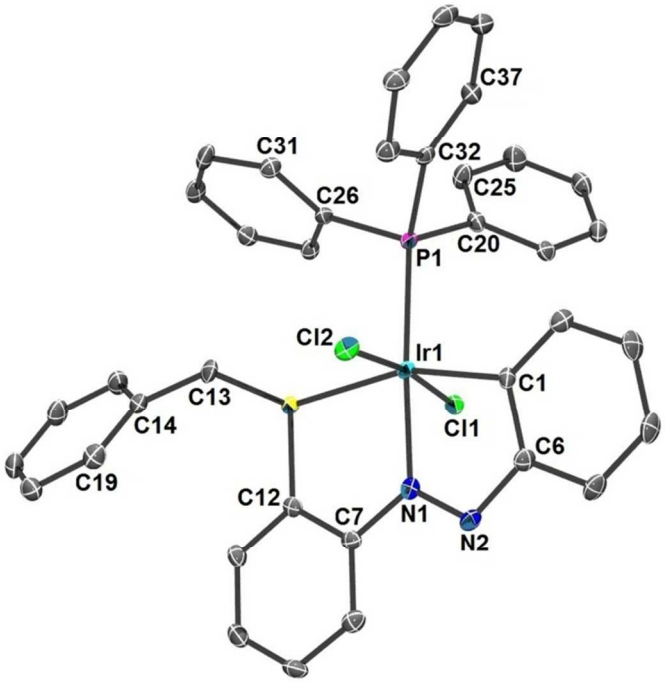

Fig. 1 ORTEP of **2a** with ellipsoids at the 40% probability level. Hydrogen atoms are omitted for clarity.

3.2CH_2Cl_2. The unit cell of **3** consists of $[Ir(L^S)Cl(PPh_3)_2]$ neutral molecules, with dichloromethane as solvate. The complex is distorted octahedral with the central iridium(III) surrounded by the tridentate dianionic ligand (C^N^S) as well as two *trans*-PPh_3 and one chloride ion. The metal center along with the ligands $([L^S]^{2-}$ and $Cl^-)$ lie on a crystallographic plane indicating the C_s symmetry of **3** (Fig. 2).

A number of dissimilarities have been observed between the thioether **2a** and the thethiolato **3**, notably: (i) Ir1−S1(thioether) distance is longer by 0.04 Å than the analogous Ir1−S1(thiolato) distance, indicating enhanced bonding ability of the latter; (ii) Ir1−N1(trans to π-acid ligand PPh_3) length of **2a** is

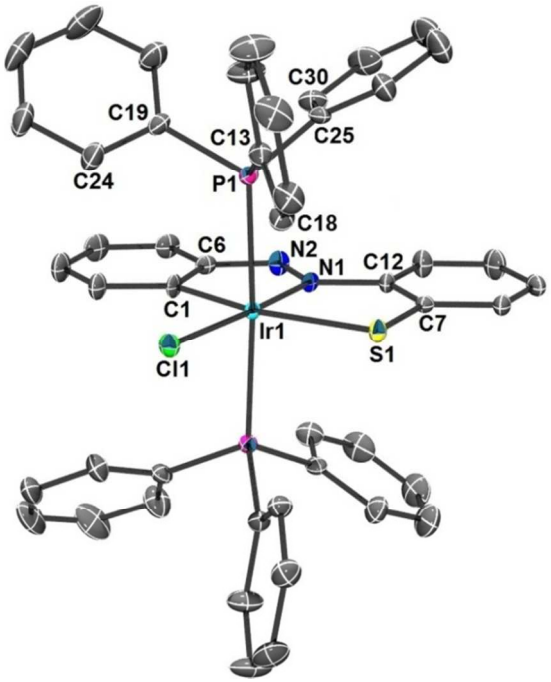

Fig. 2 ORTEP of **3** with ellipsoids at the 40% probability level. Hydrogen atoms are omitted for clarity.

significantly longer (~0.05 Å) than Ir1−N1(trans to chloride ligand) length of **3**, which is consistent with the superior overlap of the PPh_3 d/σ* orbital with metal-d orbital compared to the poorer overlap between

Table 1 Selected Metrical Parameters for **2a**, **3**, **4** and **5b**

Bond parameter	Compounds			
	2a	**3**	**4**	**5b**[§]
Ir1–C1	2.025(5)	2.036(4)	2.045(5)	2.010(13)
Ir1–N1	2.038(4)	1.983(4)	2.004(5)	1.994(12)
Ir1–S1	2.434(1)	2.475(2)	2.356(1)	2.427(3)
Ir1–P1	2.326(1)	2.388(2)	2.389(1)	2.281(3)
Ir1–Br1				2.552(1)
Ir1–Cl1	2.361(1)	2.407(2)	2.380(2)	2.383(3)
Ir1–Cl2	2.362(1)			
N1–N2	1.275(5)	1.308(5)	1.274(6)	1.243(16)
S1–O1			1.459(2)	

[§]average distance

chloride-d and metal-d orbitals; (iii) N1−N2 azo distances in coordinated thioether, thiolato, and free ligand[9] are 1.275(5), 1.308(5), and 1.251(3) Å, respectively, symptomatic of that significant Ir^{III}(5d)→N(azo π*) back-bonding occurs in thiolato **3** and such back donation severely impedes in presence of π-acceptor PPh_3 ligands in the trans position of **2a**; (iv) Ir1−P1(trans to azo) length of **2a** is significantly shorter by *ca.* 0.06 Å than Ir1−P1(trans to PPh_3 ligand) length of **3** and this event is a clear indicative of the π-acidity order: PPh_3 >

azo); (v) Ir1−Cl1 (trans to chloride) average length of **2a** is significantly shorter by ca. 0.05 Å than Ir1−Cl1(trans to azo) length of **3** (trans influence order: azo > chloride); and (vi) the N, S chelate bite angle of the bianionic ligand $[L^{S}]^{2-}$ of **3**, 83.73(11)°, is marginally larger than that of the monoanionic ligand $[L^{SCH_2Ph}]^{-}$ of **2a**, 83.07(11)°.

4.CH_2Cl_2. The sulfinato complex **4** is somewhat similar to that of the thiolato **3.** Both of them crystallize in *Cmc*2_1 space group indicating the presence of a crystallographic mirror that passes through the metal and anionic ligands, thereby bisecting the O−S−O angle. The coordination environment of **4** is exactly similar to that of **3** with the only disparity of the dioxygenated thiolato-S center (Fig. 3). Coordination of the oxidized sulfur leads to significant changes in the bonding pattern primarily within the tri-coordinated ligand as compared to that in **3**. Noteworthy features include (i) Ir1−S1(sulfinato) length is radically shortened by 0.12 Å than the analogous Ir1−S1(thiolato) bond of **3**, symptomatic of the coordination of oxidized sulfur with Ir(III), (ii) slight decrease ca. 0.03 Å of N−N (azo) distance of **4** relative to **3** is indicative of moderate impediment of Ir^{III}(5d)→N(azo π^*) back-bonding. This can be rationalized by the reduced of π-donor ability induced by S−oxygenation *via* the drifting of π electron of t_2-rich iridium toward the SO_2 moiety, thereby decreasing $Ir^{III}\rightarrow N_{azo}$ back-bonding efficacy in presence of traditional π-acceptors.[1c,16f,18b,20c] Notably, the other metrical parameters within the coordination sphere *viz*. Ir−C, Ir−N, Ir−Cl and Ir−P are found to be practically unaffected in **3** and **4** (Table 1), signifying that there occurs only minor perturbations around the

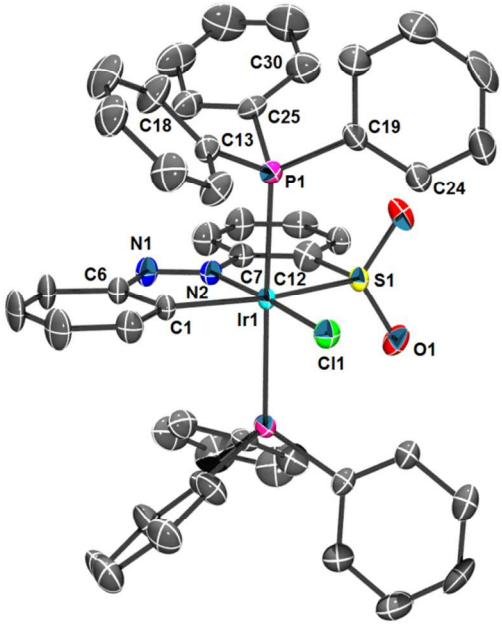

Fig. 3 ORTEP of **4** with ellipsoids at the 40% probability level. Hydrogen atoms are omitted for clarity.

iridium centre during the course of thiolato to sulfinato transformation. Significant decreased of Ir1–S1 length in the sulfinato **4** as compared to its thiolato analogue **3** can be ascribed to the following effects: (a) decreased e–e repulsion between the Ir-t_2 and the nonbonding π-donor/out-of-plane S_{3p} orbital of thiolato function upon oxidation (b) the contracted radius of the oxidized sulfur (SO_2Ar) as compared to the thiolate sulfur (*S*Ar) *vis-à-vis* increased ionic interaction between iridium and sulfinato-S, (c) $Ir^{III}(t_2) \rightarrow SO_2(\pi^*)$ back donation.[16f,18b,19a,23] The plausible $Ir^{III}(t_2^6) \rightarrow SO_2(\pi^*)$ back-donation in **4** can be nicely substantiated with the theoretical analysis (Fig. 4). The optimized Ir–S bond in sulfinato **4** (2.473 Å) is 0.05 Å shorter than the computed Ir–S bond in **3** (2.520 Å), reproducing the trend observed in the crystal structures. Moreover, a slight decrease in calculated N–N azo length in **4** (by 0.02 Å) relative to **3** signifies that the $Ir^{III}(t_2^6) \rightarrow$ azo-π* back-bonding becomes less important in former complex. The S–O distance for the sulfinato, S1, of 1.459(2)

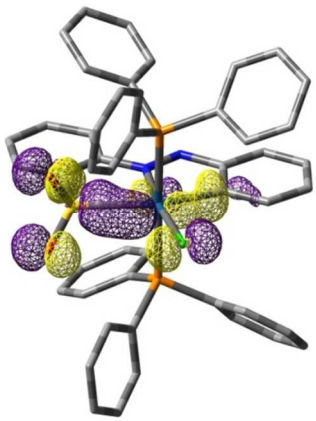

Fig. 4 Illustration of $Ir^{III}(d_{xy}) \rightarrow SO_2(\pi^*)$ back-donation in HOMO of **4**.

Å lie in the usual range (1.42-1.48 Å)[18b,d] with the O–S–O angle Å 113.4(2)° and O···O nonbonding distance 2.435 Å.

5b. The complex crystallizes in $P2_1$ space group with two molecules in the asymmetric unit ($Z' = 2$). Diffraction study authenticates the formation of S–C(alkyl) bond in **5b** and it has been to be isomeric with **2**, except for the nature of halides (Fig. 5). It is worth mentioning that the halide ion of the reactant alkyl halide (CH_2CHCH_2Br) enters into the trans position relative to PPh_3.

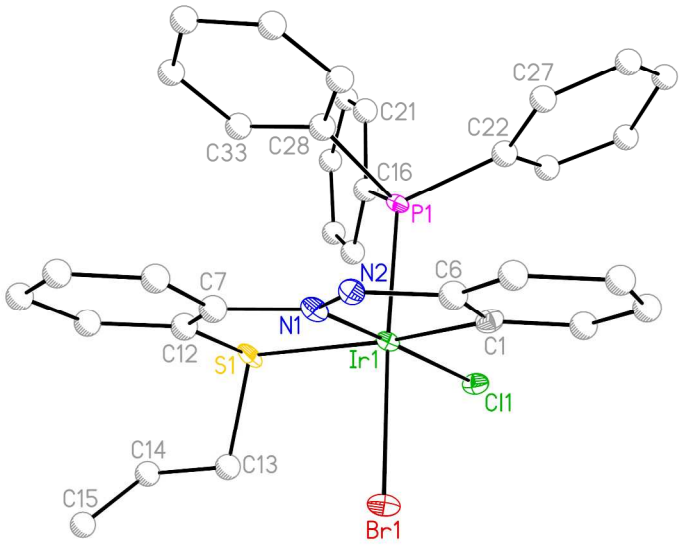

Fig. 5 Molecular view and atom labeling scheme of **5b**. Hydrogen atoms have been omitted for clarity.

Ground State Geometries and Frontier Molecular Orbital Compositions

The optimized geometries and partial MO diagram of **2a**, **3** and **4** are shown in the ESI (Fig. S2-S3†), and the significant metrical parameters are listed in Table S2†. Isodensity plots of some selected orbitals of the complexes are depicted in Fig. 6. The partial FMO compositions of the complexes are listed in Table S3-S5† in the ESI and energy levels of few selected orbitals along with HOMO−LUMO energy gap are displayed in ESI (Fig. S4†). Significant changes of FMOs and alteration of orbital composition are apparent during the modification of sulfur center of the ligand and the noteworthy features can be summarized as: (i) energies of HOMO of **2a** and **4** are appreciably stabilized than that of **3** and this can be rationalized by the considerable incorporation of out of plane nonbonding S_{3p} (~50%) into HOMO of **3**. (ii) The contribution of metal 5d in HOMO of these compounds varies appreciably and gradually increases in the sequence: **3** (10%) < **4** (18%) < **2** (42%). Minimal involvement of metal in HOMO for **3** is consistent with the ligand-center oxidation description in the redox process. (iii) Unlike **2** and **3**, a strong σ interaction is found between iridium $5d_{zx}$ and π* $S(=O)_2$ moiety in **4** as evident from its HOMO (Fig. 4).[16f,18b,19a,23] (iv) Appreciable decrease in the HOMO−LUMO gap in **3** relative to others (Fig. S4†) is associated with the bathochromic shift of the lowest energy UV-vis excitation.

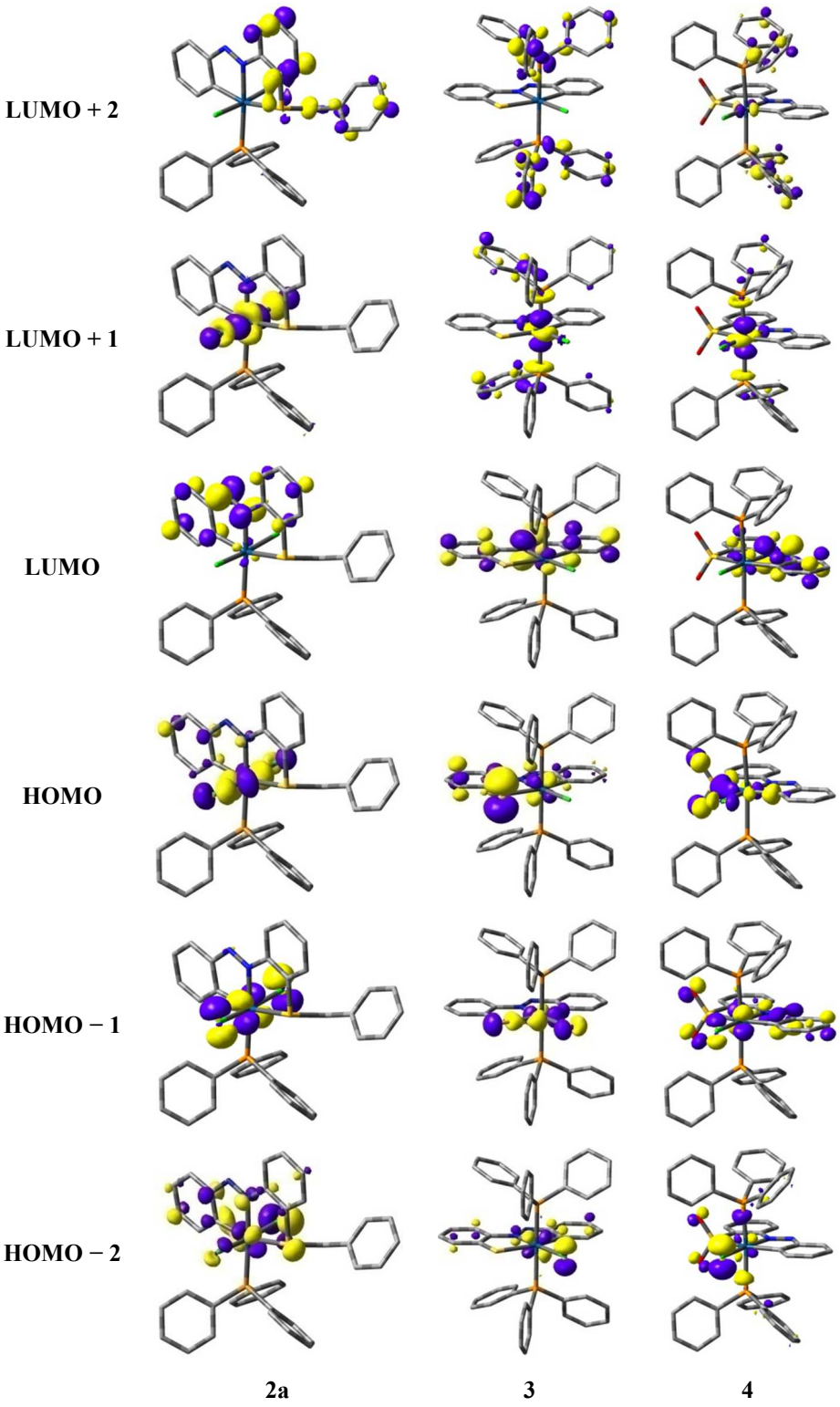

Fig. 6 Isodensity surface plots of some selected frontier molecular orbitals for the complexes **2a**, **3** and **4** at their optimized S_0 geometry in gas phase. Isodensity value 0.05 e $Bohr^{-3}$.

Ligand Redox and EPR

Electron-transfer property of the organosulfur iridium(III) complexes was studied by using cyclic voltammetry in 1:1 dichloromethane/acetonitrile solution (0.1 M NEt_4ClO_4) by using a platinum working electrode at 25°C (Table 2). The reported potential is referenced to the Ag/AgCl electrode. The value for the ferrocenium–ferrocene couple, under our experimental conditions, was 0.51 V. The one-electron nature of the redox couples has been verified by comparing the current height (i_{pa}) with that of the standard ferrocene–ferrocenium couple under identical experimental conditions.

Table 2 Electrochemical Data of Compounds[a] measured *vs* Ag/AgCl reference electrode in acetonitrile

Compound	$E_{1/2}$/V (ΔE_p/mV)
2a $[Ir(L^{SR})Cl_2(PPh_3)]$	−1.28,[b]
3 $[Ir(L^{S})Cl(PPh_3)_2]$	−1.30,[b] +0.75(82)
4 $[Ir(L^{SO_2})Cl(PPh_3)_2]$	−1.20,[b]
5b $[Ir(L^{SR})ClBr(PPh_3)]$	−1.29,[b]

[a] Solute concentration ≈ 10^{-3} mol dm^{-3}; scan rate, 50 mV s^{-1}; $E_{1/2} = 0.5(E_{pa} - E_{pc})$ for reversible one-electron process, where E_{pa} and E_{pc} are the anodic and cathodic peak potentials, respectively $\Delta E_p = E_{pa} - E_{pc}$. [b] E_{pc} = cathodic peak potential value.

Unlike all other organosulfur compounds of iridium(III), the mononuclear **3** exhibits a reversible oxidative response at $E_{1/2}$ = +0.75 V *vs* Ag/AgCl, characterized by a rather small peak-to-peak separation ($\Delta E_p = E_{pa} - E_{pc}$ = 82 mV) (Fig. 7) and such response is absent in the other organosulfur compounds of iridium(III). This observation suggests that the concern redox orbital is primarily associated with the thiolato-S centre and derivatization at thiolato-S eradicates this response. Ligand center nature of the oxidative wave

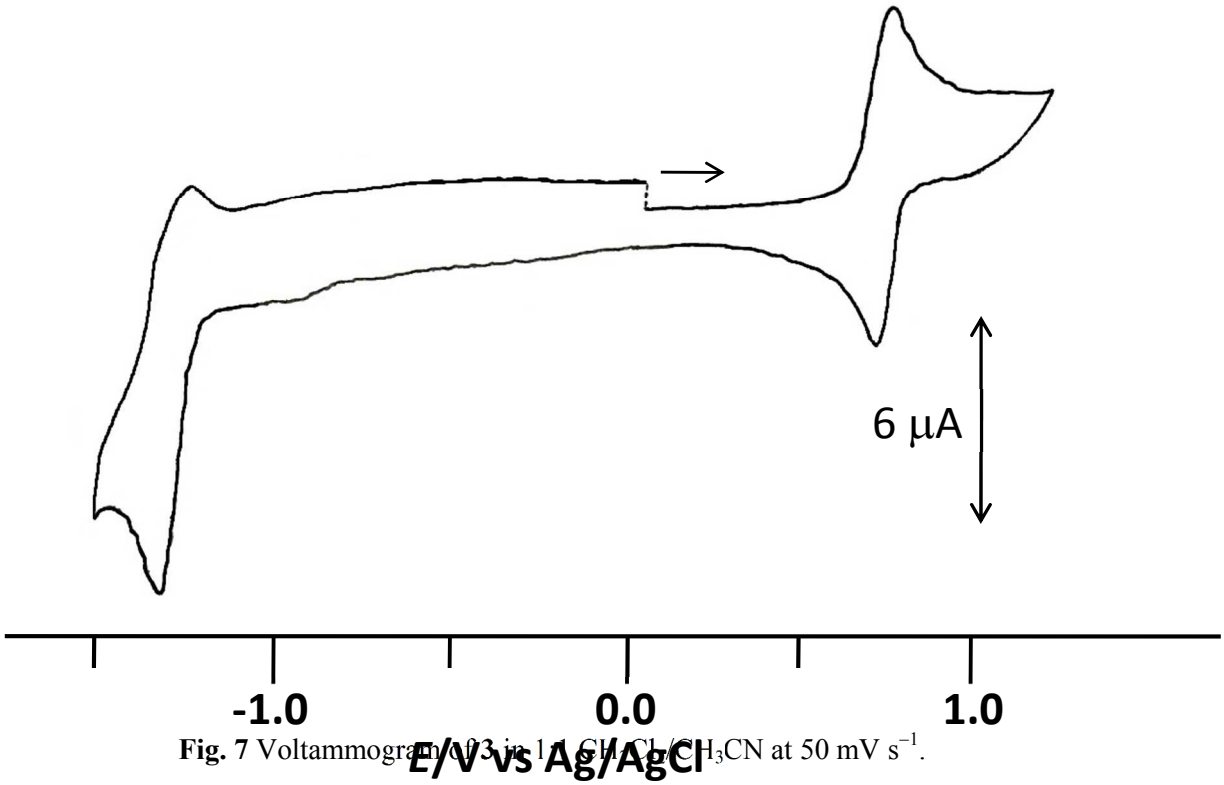

Fig. 7 Voltammogram of **3** in 1:1 CH_2Cl_2/CH_3CN at 50 mV s^{-1}.

is further supported by the observation that the corresponding rhodium analogue[9] shows alike oxidative couple with merely a difference of 0.07 V. Notably, the redox response for typical metal center oxidation process usually differs by ~0.2 V for analogous complexes of 4d and 5d series for a given group due to relativistic destabilization of valance d in case of third transition complex.[28] Redox noninnocence of the thiophenolato function in the mononuclear species is substantiating by the EPR and theoretical studies. The compound **3** is susceptible to the facile electrochemical as well as chemical oxidation. Coulometric study at 300 K confirms the oxidation to be a one-electron process and demonstrates a fully reversible $\mathbf{3}^{\bullet+}/\mathbf{3}$ couple. It is very likely that this process corresponds to the oxidation of the thiophenolate sulfur atom, yielding a iridium-bound thiyl radical (eq 1).[12-14]

$$[Ir^{III}(L^{S-II})Cl(PPh_3)_2] - e^- \leftrightarrow [Ir^{III}(L^{S-I})Cl(PPh_3)_2]^+ : \qquad E_{1/2} \qquad (1)$$

Similar type of reddish brown oxidized species is observed upon addition of conc. sulfuric acid to the dichloromethane solution of **3**. The oxidized compound obtained by both the methods displays complex EPR spectra with *g* values close to 2.0 in fluid solution (Fig. 8). The structured feature of the EPR signal signifies somewhat axial nature of the spectra and this can be attributed to the participation of metal orbital into the magnetic orbital.

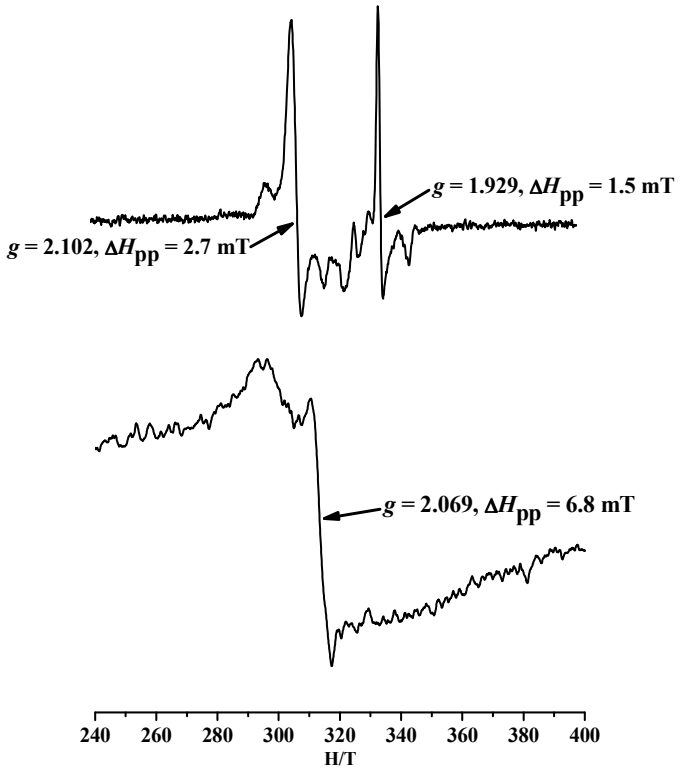

Fig. 8 X-band EPR spectrum of $\mathbf{3}^{\bullet+}$ in CH_2Cl_2 in presence of conc. H_2SO_4 at 300 K (Instrument settings: microwave frequency, 9.063 GHz; microwave power, 0.998 mW; modulation frequency, 100 kHz) (top), electrochemically generated $\mathbf{3}^{\bullet+}$ in CH_3CN at 300 K (Instrument settings: microwave frequency, 9.064 GHz; microwave power, 2.000 mW; modulation frequency, 100 kHz) (bottom).

The overall intense feature of the spectra, indicated by a rather small ΔH_{pp} values, with small anisotropic nature implies the petite contribution of iridium-d to the spin-bearing orbital.[29] It has been found that most of the reported six coordinated metal stabilized thiyl radical species contain metal atom possessing half or full filled t_2 configuration and we believe that the thiyl radical in the one-electron oxidized form $\mathbf{3}^{\bullet+}$ is stabilized by coordination to a kinetically inert Ir^{III}-t_2^6 center. All the complexes exhibit one-electron irreversible reductive wave near −1.3 V *vs* Ag/AgCl. These responses are believed to be centered on the terdentate ligand with substantial contribution of the azo moiety (Fig. 6).

To gain insight into the nature of the redox orbitals, we performed DFT calculation by optimizing the geometry of **2**−**4** at B3LYP/(6-31G + LANL2DZ) level. Calculation indicates that HOMO for **3** is the most destabilized one among the other organosulfur compounds and mainly delocalized over the phenylthiolato framework with an appreciable contribution from S_{3p} (49%) and phenyl (34%) along with Ir-d_{xz} (10%) while LUMO is exclusively constituted of azo-π* (45%) and phenyl-π* (43%) of the ligand. Accordingly, the

oxidative response of **3** is ascertained to be the 3p orbital of thiolato-S (eq 1). It is worth noting that the absence of reversible oxidative response for other complexes is nicely corroborated with the insignificant contribution of nonbonding out-of-plane S_{3p} orbital in the respective HOMO of **2a** and **4**. Comparison of the optimized geometry of **3** and $\mathbf{3}^{\bullet+}$ species reveals that structures of both are comparable except to the marked shortening of Ir–S bond length by 0.09 Å and moderate lengthening of Ir–P bond by 0.05 Å in $\mathbf{3}^{\bullet+}$. Analysis shows that the metal-d and PPh_3 contributions are enhanced by 5% and 10% respectively along with a reduction of S_{3p} by 25% in HOMO of $\mathbf{3}^{\bullet+}$ relative to that of **3** (Table S6†). The most appropriate formulation of the one-electron paramagnetic $\mathbf{3}^{\bullet+}$ can be described as $[Ir^{III}(L^{S-I})Cl(PPh_3)_2]^{\bullet+}$ where the unpaired spin is delocalized mainly over phenylthiolato(π) ring (S_{3p} 24% and phenyl-π 43%) with significant involvement of Ir-d_{zx} (15%) orbital (Fig. 9). Similar computational study on the rhodium analogues reveals more or less same feature except for the relatively poor involvement of Rh-d in HOMO (Table S6†) and this is no exception from the usual trend of lower participation of 4d as compared to that of 5d. This description is nicely substantiated with the observed g value, which is typically that of free-electron. The small axial nature of the observed EPR spectra is a clear indication of the delocalization of some part of the electron spin from the thiophenolato ring toward iridium.[29] Notably, metal contribution is more pronounced in iridium complex relative to the rhodium analogue (Table S6†) and this phenomenon can be attributed to the higher spin-orbit interaction of iridium (spin-orbit coupling constant, ξ = 3909 cm^{-1}).[30] The net spin density of one-electron oxidized form $\mathbf{3}^{\bullet+}$ (ρ_S = +0.543, ρ_{Ph} = +0.315, ρ_{Ir} = +0.151) is depicted in Fig. 9, unambiguously demonstrates the essentially thiophenolato-based oxidation with a little involvement of Ir-t_2. Ligand centered electrochemical responses *vis-à-vis* stability of metal-bound thiyl radical complex reveal the redox noninnocent nature of the phenyl-azo-thiolato ligand.

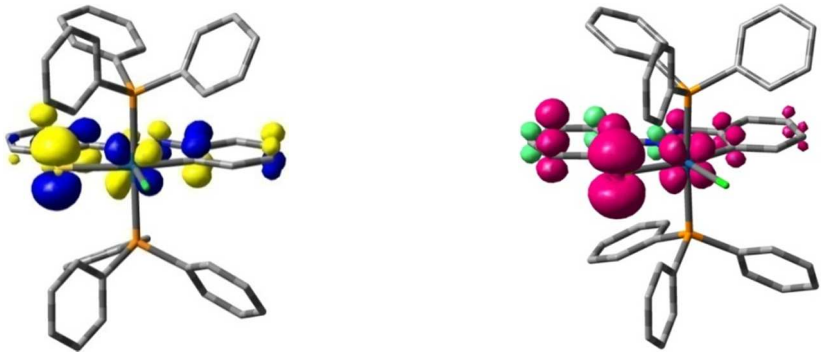

Fig. 9 Isodensity surface plot of SOMO (left) and net spin density of the one-electron oxidized thiyl radical $\mathbf{3}^{\bullet+}$. Isodensity value 0.003 e $Bohr^{-3}$.

In contrast, the components of LUMOs of all the complexes are essentially identical in nature and comprise exclusively azo-π* and phenyl-π* of coordinated organosulfur ligand with practically no participation of S orbitals. Accordingly, irreversible reductive responses can be attributed to the coordinated ligand (primarily azo moiety) reduction (Fig. 6).

Spectroscopic Properties

IR Spectra

The complexes exhibit several sharp and strong vibrations within 1600-400 cm^{-1} in the Infrared spectra. The bands near 1430 cm^{-1} are assigned to the ν_{NN} for all the complexes and they are at somewhat lower energy region relative to that of the free ligand, HL^{SCH_2Ph} (ν_{NN} 1453 and 1492 cm^{-1})[28], plausibly due to the Ir(III)-d $\rightarrow$ azo-π* back-bonding. Theoretical study reveals that the dominant features near 1370 and 1400 cm^{-1} in all the three types of compounds are attributable to N–N stretching. Strong features near 520 and 690 cm^{-1} are indicative of metal-phosphine bonding. A pair of additional intense features at 1042 and 1161 cm^{-1} was observed in the case of **4**, presumably due to the stretching in Ir−$S(=O)_2$ moiety (Fig. S5 in the ESI†).[1c,16a,e,19d] The significant frequencies of **2**−**4** have been assessed at B3LYP/(6-31G + LANL2DZ) level of theory and listed in ESI, Table S7†. A good qualitative agreement is achieved between theory and experiment and hence no attempt has been made to scale the computed data. The ν_{IrP} vibrations of the compounds are calculated in the region ~430–550 cm^{-1}. It is noteworthy that these modes are mixed with ν_{PC} stretching and δ_{PC} deformation modes. The computed symmetric and asymmetric S–O stretches are found near 975 and 1100 cm^{-1} respectively (with the difference of ~120 cm^{-1}) and it is fairly consistent with the observed data.

NMR

All the complexes gave satisfactory elemental analyses and have been found to be diamagnetic, which corresponds to the trivalent iridium (t_2^6, $S = 0$). All the reported neutral organoiridium(III) sulfur complexes are soluble in both non-polar and polar organic solvents such as benzene, toluene, chloroform, dichloromethane, acetone, acetonitrile and so on. ^{1}H NMR spectra are depicted in the ESI, Fig. S6-S7†. Absence of alkyl resonance in the ^{1}H NMR spectrum of iridium(III) thiolato complex **3** authenticates the occurrence of S-dealkylation. The alkyl proton signals of thioether compounds **2a** and **2b** appeared as a doublet at δ 6.1 (SCH_2Ph, $^1J_{HH}$ = 7.8 Hz) and a singlet at δ 3.2 (SCH_3) resonances, respectively. The ^{31}P NMR spectra of the complexes **3** and **4** display only a singlet resonance in spite of the presence of two phosphine groups, this is indicative of the presence of magnetically equivalent phosphine environment i.e., they are disposed trans to each other (Fig. S8†). The NMR and MASS spectral studies of **3**, unequivocally established its substantial stability in solution (Fig. S9† in the ESI).

Absorption Spectra

Electronic spectra of organoiridium(III) sulfur compounds were recorded in dichloromethane at room temperature. The UV-vis spectra of **3** and **4** along with their respective theoretical spectra are depicted in Fig. 10 and that of **2a** is presented in ESI (Fig. S10†). There are multiple low-energy transitions and these excitations are primarily due to charge-transfer transitions within the phenyl-azo-sulfur ligand with different amounts of metal-d participation. The spectral patterns of **2–4** are comparable except for the fact that greater numbers of transitions are observed in the lower energy region of **3**. To gain deeper insight into the electronic properties of the transitions involved in the optical absorption processes, we have investigated the complexes by means of time-dependent density functional theory (TD-DFT) in CH_2Cl_2 solvent using CPCM model (see Computational Method for details). The computed vertical transitions were calculated at the equilibrium geometry of the S_0 state and described in terms of one-electron excitations of molecular orbitals of the corresponding S_0 geometry. The most relevant transitions involved along with their energy, character, oscillator strengths computed in solvent and their assignments as well as experimental results of compounds **2a, 3** and **4** are listed in the ESI (Table S8-S10†). The calculated transitions with moderate intensities ($f \geq 0.02$) can be envisaged.

For **3**, the HOMO, HOMO − 1, HOMO − 2 and HOMO − 3 have been scrutinized and these involve exclusively the delocalized π orbitals encompass over azo-thiolato ligands, along with substantial participation of metal-d. The HOMO is mainly composed of S_{3p} (~50%) and Ph_{π}[§] (34%) in addition to minor contribution of Ir-d_{zx} (10%). In contrast, HOMO – 1 has been found to be Ir-d_{xy} (36%) with comparable

[§] Ph_{π}/Ph reported in this work representing the phenyl ring of ligand **1**.

contributions from S_{3p} and Cl_{3p} (~24% each). The HOMO – 2 comprises of Ph_{π} (37%) and Cl_{3p} (22%) along with Ir-d_{zx} and phosphine-π whereas the HOMO – 3 is mainly of Ph_{π} (60%) with significant contribution from Ir-d_{yz} (19%) and phosphine-π (12%). In contrast, LUMO is an exclusively π* orbital delocalized mostly over azo and phenyl ring (~44% each) of the ligand. The LUMO + 1 is principally composed of phosphine-π* (~68%) along with substantial contribution from Ir-d_z^2 orbital (~25%). The LUMO + 2 and LUMO + 3 are basically similar in nature, having almost exclusive contribution from phosphine-π* orbital.

The lowest energy transitions in the visible region appear as broad band near 733 nm in **3** and this feature is in excellent agreement with the computed band at 719 nm (1.7253 eV, f = 0.0562), which essentially consist of H → L (98%) and can be ascribed as {[3p(S) + d_{zx}(Ir)] → π*(azo)} ILCT transition admixed with a little MLCT character. The shoulder around 390 nm is in good agreement with the theoretical band at 387 nm (3.2010 eV, f = 0.0937) which basically comprises of H – 3 → L (80%) and H – 4 →L (13%), assigned to {[π(Ph) + π(PPh_3) + 3p(Cl)] → π*(azo)} LLCT/ILCT transition. The low energy

absorptions near 368 and 350 nm in the UV region agreed well with the theoretically calculated bands at 375 nm and 356 nm respectively. The first one at 375 nm (3.3034 eV, f = 0.0540) appears exclusively as H – 4 → L (80%) and can be referred to {[π(PPh_3) + 3p(Cl)] → π*(azo)} transition, whereas the latter one at 356 nm (3.4786 eV, f = 0.1638) is attributed to H – 5 → L (68%) and H – 7 → L (12%) transition, mainly due to {π(PPh_3) → [π*(azo) + π*(Ph)]}. Both the excitations are characterized as LLCT transition. The next observed higher energy transition near 278 nm is computed at 296 nm (4.1797 eV, f = 0.0454), 293 nm (4.2270 eV, f = 0.0316) and 292 nm (4.2326 eV, f = 0.1177). The former excitation can be described in terms of linear combination of H → L + 9 (62%), H – 2 → L + 1 (12%) and H – 3 → L + 1 (10%) and it is assigned to {[3p(S) + π(Ph)] → π*(PPh_3)}LLCT transition; while the second one is attributed to the combination of H – 16 → L (64%) and it is assigned to {[3p(S) + π(PPh_3) + 3p(Cl) + d_{zx}(Ir)] → π*(azo)} LLCT/MLCT transition. The last one can be assigned as {[3p(S) + 3p(Cl) + d_{xy}(Ir) + d_{zx}(Ir)] → [π*(PPh_3) + π*(azo)]} LLCT/MLCT transition with calculated contributions from H – 16 → L (24%), H – 1 → L + 4 (21%), H – 1 → L + 7 (13%) and H – 1 → L + 10 (10%). The schematic representation of the energy levels of molecular orbitals involved in the electronic transitions of **2a, 3** and **4** are depicted in the ESI (Fig. S11-S13†).

For the organoirium(III) thiolato complex **3**, the occupied FMOs show strongly mixed π character of the coordinated ligand along with moderate metal t_2 character while the virtual FMOs comprise primarily ligand π* with some admixture of iridium $5d_z^2$. In the visible region, the excitation near 733 nm can be best described as primarily singlet-manifold intra-ligand charge-transfer (^{1}ILCT), mainly π(S_{3p}) to π*(azo) within phenyl-azo-thiolato ligand, along with little contributions from Ir-d_{zx} to π*(azo) ^{1}MLCT transition. This transition is shifted bathochromically by 22 nm relative to the analogous rhodium compound.[9]

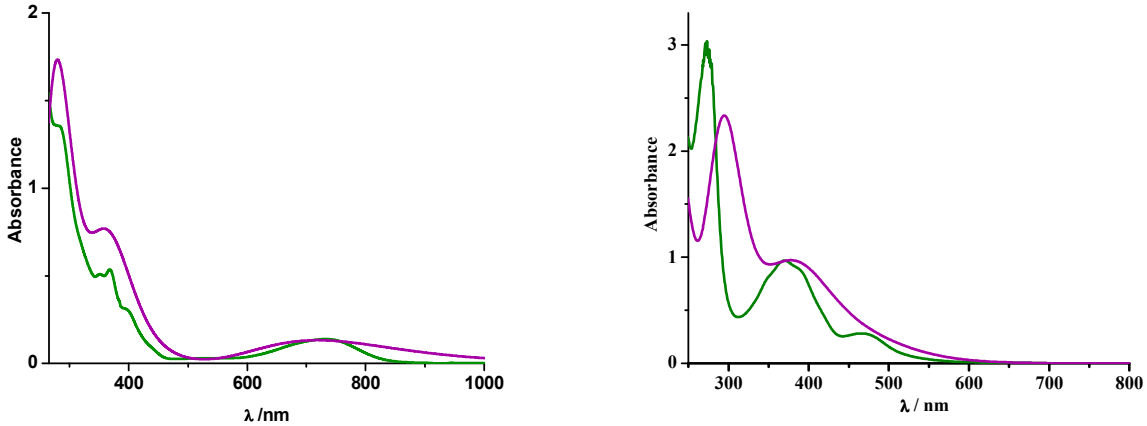

Fig. 10 Experimental (green) and theoretical (violet) absorption spectra of **3** (left) and **4** (right) in dichloromethane.

The occupied MOs (HOMO to HOMO − 3) of **2** and **4** differ appreciably as compared to that of **3**. For **2**, analogous MOs comprise mainly strongly mixed character of Cl_{3p} and Ph_{π} with extensive metal t_2 character. In contrast, these MOs of **4** exhibit noteworthy involvement of SO_2 moiety, Ph_{π}, Cl and PPh_3 with significant metal t_2 participation. Among the virtual orbitals (LUMO to LUMO + 3), composition of LUMO is alike for all the compounds and involves ~45% of each π*(azo) and π*(phenyl) of the C^N^S ligand. While the other three virtual orbitals of **2** contain strongly mixed π* of aromatic rings of ligand and PPh_3 by different extent with little participation of metal except L + 1, which is dominated by ca. 43% $5d_z^2$ character. Analogous orbitals of **4** comprise mainly the π* of PPh_3 with slight participation of metal except L + 1, which is dominated by ca. 30% $5d_z^2$ character.

In the visible region, the lowest energy excitations of **2** around 630 nm is ascribed as H → L (97%) and can be recognized by $\{[d_{zx}(Ir) + 3p(Cl)] \rightarrow [\pi^*(azo + Ph)]\}$ ^{1}MLCT admixed with ^{1}LLCT. Lowest energy transition in the UV region is observed as shoulder near 390 nm and is dominated by strongly mixed ^{1}LLCT/^{1}ILCT/^{1}MLCT character while slightly higher energy excitations near 367 and 350(sh) nm are ascribed as exclusively $\{[Ph(PPh_3) + 3p(Cl) + Ph(CH_2Ph)] \rightarrow [\pi^*(azo + Ph)]$ ^{1}LLCT/^{1}ILCT transitions. In sulfinato **4**, shoulder near 390 nm can be assigned as ^{1}LLCT admixed with ^{1}LLCT/^{1}MLCT with contributions from $\{[\pi(PPh_3) + 3p(Cl) + \pi(SO_2) + d_{xy}(Ir)] \rightarrow [\pi^*(azo + Ph)]\}$ and absorptions near 370 and 350(sh) nm are exclusively $\{\pi(PPh_3) \rightarrow [\pi^*(azo + Ph)]\}$ ^{1}LLCT in nature. While the next higher energy transition near 270 nm is basically $\{[3p(Cl) + \pi(SO_2) + \pi(Ph)] \rightarrow [d_z^2(Ir) + \pi^*(PPh_3)]\}$ ^{1}LMCT/^{1}LLCT involving metal e orbital. Unlike **2** and **4**, electronic transitions of **3** are found to be shifted toward higher energy of the spectrum indicating the occurrence of energetically more favorable transitions. This is caused by small HOMO–LUMO gap due to the involvement of nonbonding S_{3p} in HOMO.

Luminescence Spectra

The emission spectral behaviour of the organoiridium(III) sulfur complexes were studied at room temperature in dichloromethane solution. All complexes upon excitation at the wavelengths, where their ^{3}ILCT/^{3}LLCT absorption maxima were observed, exhibit broad luminescent maxima within the range 400–450 nm and these remain unaffected with the energy of excitation wavelengths. The complexes **2**–**4** are found to be moderate to strong emitters ($\Phi = 0.29 \times 10^{-1}$–$1.23 \times 10^{-1}$). Table 3 summarizes the emission maxima (λ_{em}), quantum yield (Φ), lifetime (τ), radiative (k_r) and nonradiative (k_{nr}) decay rate constants. The luminescence spectra are presented in Fig. 11 and time-resolved photoluminescence decay are depicted in ESI, Fig. S14†. Notably, luminescence study of transition metal complexes incorporating azo ligands is less known.[31]

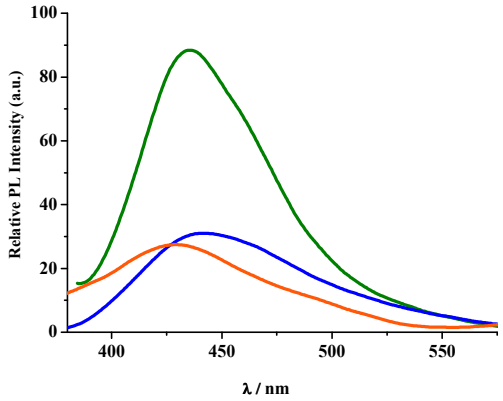

Fig. 11 Luminescence spectra of complexes **2a** (blue), **3** (green) and **4** (orange) in dichloromethane.

In order to investigate the geometrical rearrangement as well as to understand the electronic nature of the emitting excited state, geometrical optimization of the lowest lying triplet-manifold excited state (T_1) was performed by means of DFT using the unrestricted Kohn−Sham approach at (U)B3LYP/(6-31G + LANL2DZ) level. The most meaningful geometrical parameters are listed in ESI, Table S11-S13†. The isodensity surfaces of the Highest and Lowest Singly Occupied Molecular Orbitals, *viz*. HSOMO and LSOMO, of mononuclear compounds at the relaxed T_1 geometry are depicted in Fig. 12. The complexes display comparable metrical parameters for Ir−C, Ir−N, Ir−P, Ir−S and Ir−Cl linkages at the T_1 optimized geometry as well as in the S_0 state (average displacement range 0.007−0.03 Å) (Table S2† in ESI) except Ir−S (0.05 Å) of **3**, Ir−N (0.06 Å) and Ir−Cl (0.06 Å) of **4**. It is noteworthy that the N−N(azo) bond distance significantly lengthens at the T_1 optimized geometry relative to the S_0 state by 0.07−0.12 Å). The absence of appreciable distortion around iridium signifies that the population of the T_1 state results in only minor deviations in the geometrical arrangement of the coordination spheres i.e., metal-ligand interactions only

Table 3 Luminescence spectral data[a] for iridiumsulfur complexes in dichloromethane at room temperature

Compound	λ_{em}, nm	τ, ns	Φ	k_r, × 10^6 s^{-1}	k_{nr}, × 10^8 s^{-1}
1a	367	6.743	0.291	43.156	1.051
2a	442	9.101	0.031	3.406	10.647
3	436	4.328	0.123	28.419	20.263
4	439	7.066	0.029	4.104	13.741

[a]The compounds **1a**, **2**, **3** and **4** are excited at 310, 356, 367 and 370 nm respectively.

slightly altered during $S_0 \rightarrow T_1$ excitation. This is consistent with the comparable quantum yield (Φ) of the synthesized iridium(III) complexes with that of the free ligand **1a**. Nonetheless, quantum yield (Φ) is diminished in the complexes relative to the free ligand and this fact is possibly caused by the perturbation of PPh_3 and metal-t_2 in the overall LC emissive states. Quenching of luminescence in the presence of tertiary phosphine is known.[31f] The considerable geometrical variation is confined primarily to N−N(azo) linkage (elongated by ~0.1 Å) and to a certain extent in some other iridium−ligand bonds in the excited T_1 state (ESI,

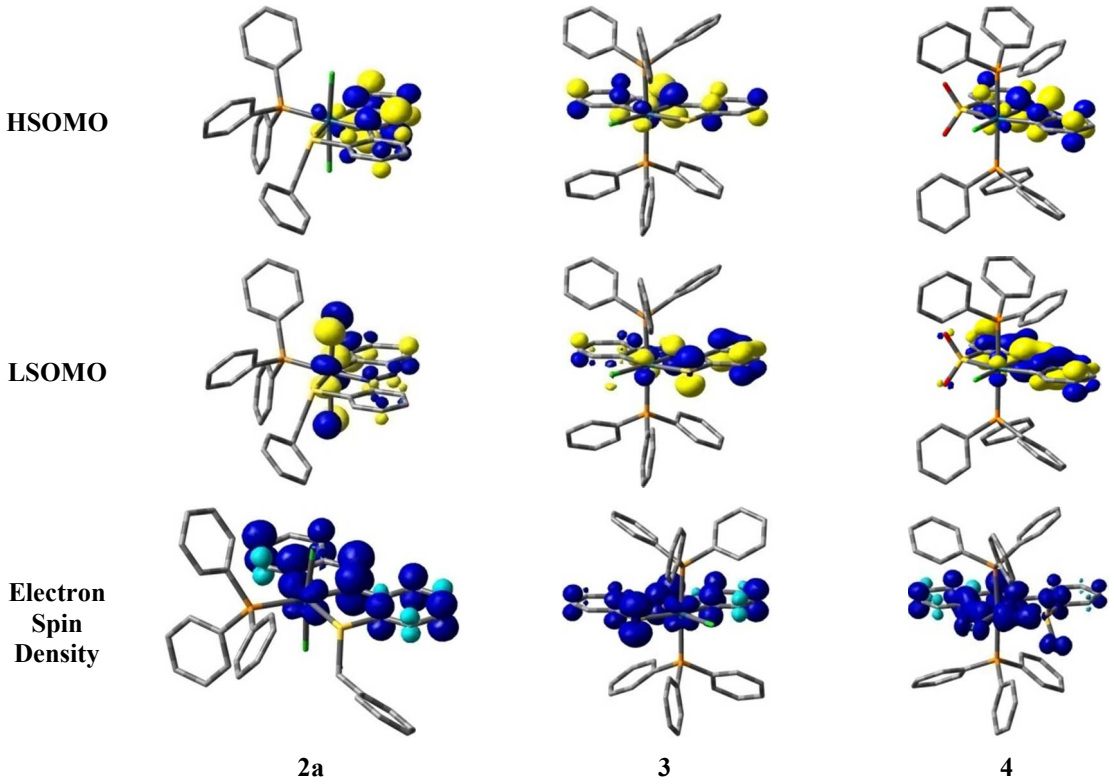

Fig. 12 Isodensity surface plots of the highest and lowest singly occupied molecular orbitals, HSOMO and LSOMO, respectively, along with the corresponding electron spin density for compounds **2a**, **3** and **4** at their T_1 geometry. Blue and turquoise colors show regions of positive and negative differences between the alpha and the beta electron densities respectively.

Table S2†). This can be ascribed to the drifting of electron density from iridium-t_2 along with S atom for **2** and the phenyl as well as S/SO_2 moiety of ligand for **3** and **4** respectively towards the azo moiety in the $^3T_1$ state.

Upon analyzing the singly occupied molecular orbitals at the relaxed T_1 geometry for thiolato **3** it was found that HSOMO assumes exclusively π(azo + Ph) while that of LSOMO comprises of primarily π(Ph) of ligand with some admixture of [3p(S) + π(azo)] along with minor contribution from metal t_2 (ESI, Table S12†). Out of these singly occupied MOs, HSOMO resembles nicely with the LUMO of the corresponding S_0 equilibrium geometry (Table S4†). Though there is no precise analogue of LSOMO at S_0 state, HOMO of the corresponding S_0 equilibrium geometry appears somewhat closer to it. Notably, the electron spin density plots for organoiridium(III) sulfur complexes disclose that the spin is located mainly on the coordinated ligand (Fig. 12).

The luminescent band of the thiolato **3** in experimental spectrum at 435 nm is computed at 427 nm (2.8974 eV, f = 0.0307) with significant transition having 216 → 211 (24%), 211 → 209 (22%), 214 → 211 (11%) character. This can be assigned exclusively to {π*(PPh_3) → [π(azo) + π(Ph) + 3p(S) + d_{yz}(Ir)]}

LLCT/ILCT/^{3}LMCT transition. Similarly, for thioether **2** the experimental emission spectrum (λ_{em} = 442 nm) is computed at 415 nm (2.9866 eV, f = 0.0164) with 175 → 173 (79%) character. This can be assigned mostly to {[π*(azo) + π*(Ph)] → [d_{xy}(Ir) + 3p(Cl)]} ^{3}LMCT transition mixed with LLCT/ILCT nature. The analogous band present in the experimental emission spectrum (λ_{em} = 438 nm) of sulfinato **4** complex is computed at 454 nm (2.7260 eV, f = 0.0208) with 218 → 196 (80%) character. This can be assigned mainly to {d_{xy}(Ir) → [3p(Cl) + π(PPh_3)]} ^{3}MLCT transition.

The plots of frontier molecular orbitals associated with the emissions of orgasnosulfur compounds of iridium(III) are presented in Fig. S15† in the ESI. The most relevant transitions involved along with their energy, character, oscillator strengths computed in solvent and their assignments as well as experimental results of iridiumsulfur compounds are listed in the ESI (Table S14†).

Experimental Section

Syntheses

General. All syntheses were performed under normal aerobic conditions unless otherwise specified**.** Solvents were dried by standard methods and distilled under argon prior to use. Ligands[32] HL^{SR} (R = Me, CH_2Ph and Ph) and complex $[IrCl(PPh_3)_3]$[33] used in this work have been synthesized following the methods previously described.

Materials. The chemicals used were purchased from the following sources: 2-aminothiophenol, 2-(Methylmarcapto)aniline, triphenylphosphine, triphenylarsine, methyl iodide, allyl bromide and $IrCl_3{\cdot}3H_2O$ from Aldrich Chemical Company. All solvents were purchased from Merck, India and dried before use according to standard methods.

Syntheses of Complexes. $[Ir(L^{SR})Cl_2(PPh_3)]$ 2, **$[Ir(L^{S})Cl(PPh_3)_2]$ 3** and **$[Ir(L^{SO_2})Cl(PPh_3)_2]$ 4.** A mixture of **1a** (R = CH_2Ph), (95 mg, 0.312 mmol), $IrCl_3{\cdot}3H_2O$ (100 mg, 0.104 mmol) and triphenylphosphine (0.22 g, 0.832 mmol) in ethanolic (50 ml) solution were heated to reflux for 24 h till the color of the solution turns to dark greenish brown. The solvent was removed under reduced pressure. Upon chromatographic purification of the solid on neutral silica gel, three fractions were eluted sequentially: (1) dark-green, **3** eluted first with 1:3 hexane-toluene mixture, followed by (2) a greenish-brown fraction corresponding to **2a** eluted with 1:20 acetonitrile-toluene mixture and (3) an orange fraction eluted with 1:10 acetonitrile-toluene mixture **4**. The chromatographically separated fractions were concentrated and dried in vacuum. Yield: (42%) for **3**; (27%) for **2b**; and (11%) for **4**. Analogous reaction with **1b** (R = Me) under identical condition afforded **2a**, **3** and **4** in 24, 39 and 9% yield respectively. For compound **2a**: FT-IR (KBr, cm^{-1}): 1433 (ν_{NN}), 693 and 518 (ν_{IrP}). ^{1}H NMR (300 MHz, $CDCl_3$): δ 6.28 (d, J = 7.8 Hz), 6.899–7.461 (m), 7.69 (d, J = 7.5 Hz), 7.84(m), 8.23 (d, J =7.2 Hz), 8.39 (d, J = 8.2 Hz). ^{31}P NMR ($CDCl_3$): δ -14.91 (s). Elem. Anal. Calcd (%) for **2a**, $C_{37}H_{30}N_2PSCl_2Ir$: C, 53.62; H, 3.65; N, 3.38. Found: C, 53.18; H, 3.72; N, 3.14. For compound **2b**: FT-IR

(KBr, cm^{-1}): 1428 (ν_{NN}), 690 and 522 (ν_{IrP}). ^1H NMR (300 MHz, $CDCl_3$): δ 3.15 (s), 6.82–7.49 (m) 7.68 (d, J = 7.4 Hz), 7.89 (m), 8.27 (d, J = 8.0 Hz). ^{31}P NMR ($CDCl_3$): δ -23.73(s). Elem. Anal. Calcd (%) for **2b**, $C_{31}H_{26}N_2PSCl_2Ir$: C, 49.47; H, 3.48; N, 3.72. Found: C, 49.18; H, 3.59; N, 3.53. For compound **3**: FT-IR (KBr, cm^{-1}): 1433 (ν_{NN}), 692 and 520 (ν_{IrP}). ^1H NMR (300 MHz, $CDCl_3$): δ 6.04 (t, J = 8.0 Hz), 6.33 (d, J = 8.4 Hz), 6.41(q), 6.65 (d, J = 7.9 Hz), 6.79 (t, J = 7.5 Hz), 7.07–7.19 (m), 7.41 (d, J = 7.7 Hz), 7.48–7.52 (m); ^{31}P NMR ($CDCl_3$): δ -14.78(s). Elem. Anal. Calcd (%) for **3**, $C_{48}H_{38}N_2P_2SClIr$: C, 59.77; H, 3.97; N, 2.90. Found: C, 59.36; H, 4.33; N, 2.72. For compound **4**: FT-IR (KBr, cm^{-1}): 1434 (ν_{NN}), 1161, 1042 (ν_{SO}), 694 and 520 (ν_{IrP}). ^1H NMR (300 MHz, $CDCl_3$): δ 6.53 (t, J = 6.98 Hz), 6.76 (t, J = 7.2 Hz), 6.93–7.18 (m), 7.42–7.50 (m), 8.01(d, J = 7.7 Hz), ^{31}P NMR ($CDCl_3$): δ -17.82(s). Elem. Anal. Calcd (%) for **4**, $C_{48}H_{38}N_2O_2P_2SClIr$: C, 57.85; H, 3.84; N, 2.81. Found: C, 57.42; H, 3.58; N, 3.02.

[Ir(L^{SR})Cl_2(PPh_3)] 2. To an ethanolic (50 ml) solution of **1a** (R = CH_2Ph), (47 mg, 0.154mmol) and $IrCl_3.3H_2O$ (50 mg, 0.142 mmol) triphenylphosphine (37 mg, 0.141 mmol) was added and heated to reflux under Ar for 4 h till a dark greenish-brown solution obtained. The resulting solution was evaporated to dryness and purified by column chromatography (neutral silica gel; CH_3CN/Toluene, 1:20). Yield: 62%.

Conversion of 2 to 3. 2a (50 mg, 0.0604 mmol) and triphenylphosphine (126 mg, 0.483 mmol) were dissolved in toluene (30 ml), and the mixture was refluxed for 20 h under Ar. Chromatographic purification was made by the above procedure. Yield: 61%. An analogous reaction with **2b** producing **3** in 55% yield.

Conversion of 3 to 4. To an acetonitrile (50 ml) solution of **3** (25 mg, 0.025 mmol) was refluxed under O_2 for 12 h till a dark orange solution obtained. Volatile organic compounds were evaporated under reduced pressure and purified by column chromatography (neutral silica gel; CH_3CN/Toluene, 1:10). Yield: 71%. Analogous reaction using aerial oxygen instead of pure O_2 for 24 h yields 64% of **4**.

[Ir(L^{SMe})ClI(PPh_3)] 5a. To a toluene (25 ml) solution of **3**, (25 mg, 0.025 mmol) methyl iodide (4.25 mg, 0.029 mmol) was added drop wise with stirring and then refluxed for 4 h till a dark orange solution obtained. The resulting solution was evaporated to dryness. Upon chromatographic purification of the solid on neutral silica gel with 1:10 acetonitrile–toluene mixture as eluent, orange red **5a** was obtained. Yield: 59%. For compound **5a**, FT-IR (KBr, cm^{-1}): 1416 (ν_{NN}), 696, 535 (ν_{RhP}). ^1H NMR (300 MHz, $CDCl_3$): δ 3.22 (s), 7. 07-7.18 (m), 7.35-7.44 (m), 7.70 (d, J = 7.4 Hz), 7.94 (d, J = 7.4 Hz), 8.01 (d, J = 7.5 Hz). ^{31}P NMR ($CDCl_3$): δ 21.86 (d, $^1J_{Rh-P}$ = 117.1 Hz). Elem. Anal. Calcd (%) for **5a**, $C_{31}H_{26}N_2PSCl_2Ir$: C, 44.11; H, 3.10; N, 3.32. Found: C, 44.50; H, 3.22; N, 3.54.

[Ir(L^{SAllyl})ClBr(PPh_3)] 5b. To a toluene (50 ml) solution of **3**, (100 mg, 0.104 mmol) Allyl bromide (14.00 mg, 0.114 mmol) was added drop wise with stirring and heated to reflux for 10 h till a dark orange solution obtained. The resulting solution was evaporated to dryness. Upon chromatographic purification of the solid on neutral silica gel with 1:20 acetonitrile–toluene mixture as eluent, orange red **5b** was obtained. Yield 62%. For compound **5b**: FT-IR (KBr, cm^{-1}): 1416 (ν_{NN}), 696, 535 (ν_{RhP}). ^1H NMR (300 MHz, $CDCl_3$): δ 4.23

(t, J = 9.4 Hz), 5.03 (q), 5.10 (t, J = 9.5 Hz), 6.43 (m), 7.08–7.33 (m), 7.51 (t, J = 9.7 Hz), 7.70 (d, J = 4.2 Hz), 8.10 (dd, J_1 = 1.6, J_2 = 1.6 Hz), 8.07 (d, J = 7.6 Hz). ^{31}P NMR ($CDCl_3$): δ -20.785(s). Elem. Anal. Calcd(%) for **5b**, $C_{33}H_{28}N_2PSBrClIr$: C, 48.15; H, 3.43; N, 3.40. Found: C, 48.54; H, 3.39; N, 3.24.

Conclusions

A novel family of orthometalated iridium(III) compounds incorporating sulfur center has been prepared following the synthesis of the organothioether **2**, *via* C(arene)–H bond activation. The most significant aspect among the syntheses is the iridium-mediated C–S cleavage product, organothiolato **3**, in the presence of PPh_3. The PPh_3 molecule acts as external stimuli and plays a vital role in the cleavage process. This provides an example of the use of foreign motivating agent during bond activation processes that may modulate the cleavage reaction in a more controlled fashion. The underlying mechanistic pathway has been established and it reveals that the cleavage reaction operates through the less common single-electron transfer (SET) mechanism. This is different from the majority of the reported platinum-metals thiolato compounds that were achieved from the thioether precursors by oxidative addition during C–S bond scission. Electrochemical study shows the facile oxidative nature of thiolato **3** in solution unlike the other organoiridium(III) sulfur compounds and the redox orbital have been resolved to be primarily the out of plane nonbonding S_{3p} orbital by computation. This accounts for the remarkable nucleophilicity of thiolato-S center as apparent from the formation of sulfur center derivatives with electrophiles like dioxygen and carbo cations. Complex **3** is very much prone to S-centered oxidation and furnishes metallosulfoxide **4** almost quantitatively *via* activation of molecular oxygen under normal aerobic condition, which provides the first instance of a iridium thilato to iridium sulfinato conversion. Facile thiolato to thioether conversion can be accomplished from the precursor thiolato **3** upon reacting with alkyl halide. These thioether complexes **5** have been found to be structurally isomeric with **2**. Finally, high electron density on the thiolato-S in **3** has been exploited to generate stable metal-bound thiyl radical species $\mathbf{3}^{\bullet+}$ in solution by chemical as well as electrochemical means. Analyses of SOMO, spin density and EPR spectra of the oxidized form of **3** authenticate the thiyl radical description and it has been concluded that both the phenyl-π as well as Ir-d play important role for the stabilization of thiyl radical $\mathbf{3}^{\bullet+}$. The organosulfur complexes of iridium(III) display rich spectral features including luminescence property and these attributions are scrutinized by DFT and TD-DFT. Scrutiny of C–S cleavage reaction using other platinum metals are currently under investigation.

Acknowledgment

Financial support received from the Department of Science and Technology (Project # SR/S1/IC-75/2010), New Delhi, is gratefully acknowledged. Mr S. Pramanik and Mr T. Ghorui thank the UGC, New Delhi and Ms S. Roy thanks DST, New Delhi for research fellowship. We are also thankful to the Department of

Science and Technology, New Delhi, India for the data collection on the CCD facility setup (Jadavpur University). We also acknowledge CAS, Department of Chemistry, Jadavpur University and the DST-PURSE program for other facilities.

† Electronic supplementary information (ESI) available: Experimental details, Analytical and spectroscopic data of new compounds. CCDC 1046498–1046501. For ESI and crystallographic data in CIF or other electronic format see DOI:

References

(1) (a) L. Wang, W. He and Z. Yu, *Chem. Soc. Rev*., 2013, **42**, 599–621; (b) S. G. Modha, V. P. Mehta and E. Van der Eycken, *Chem. Soc. Rev*., 2013, **42**, 5042–5055; (c) M. Tamura, K. Tsuge, A. Igashira-Kamiyama and T. Konno, *Inorg. Chem*., 2011, **50**, 4764–4771; (d) K. Ray, S. D. George, E. I. Solomon, K. Wieghardt and F. Neese, *Chem. Eur. J*., 2007, **13**, 2783–2797; (e) A. Magistrato, P. Maurer, T. Fässler and U. Rothlisberger, *J. Phys. Chem. A*, 2004, **108**, 2008–2013; (f) A. L. Sargent and E. P. Titus, *Organometallics*, 1998, **17**, 65–77.

(2) (a) T. A. Atesin, S. Kundu, K. Skugrud, K. A. Lai, B. D. Swartz, T. Li, W. W. Brennessel and W. D. Jones, *Organometallics*, 2011, **30**, 4578–4588; (b) H. Huang, J. Li, C. Lescop and Z. Duan, *Org. Lett.*, 2011, **13,** 5252–5255; (c) S. S. Oster, M. R. Grochowski, R. J. Lachicotte, W. W. Brennessel and W. D. Jones, *Organometallics*, 2010, **29**, 4923–4931; (d) M. R. Grochowski, W. W. Brennessel and W. D. Jones, *Organometallics*, 2009, **28**, 2661–2667; (e) R. J. Angelici, in *Encyclopedia of Inorganic Chemistry*, ed. R. B. King, Wiley, New York, 2nd edn, 2005, **3**, 1860–1877; (f) J. B. Chen and R. J. Angelici, *Coord. Chem. Rev*., 2000, **206**, 63–99; (g) C. Bianchini, A. Meli, F. Vizza, *J. Organomet. Chem*., 2004, **689**, 4277–4290; (h) D. Stirling, *The Sulfur Problem: Cleaning up Industrial Feedstocks*, RSC Clean Technology Monographs, 2000.

(3) (a) S. Kundu, B. E. R. Snyder, A. P. Walsh, W. W. Brennessel and W. D. Jones, *Polyhedron*, 2013, **58**, 99–105; (b) S. Mandal, S. Roy and S. Goswami, *Indian J. Chem*., 2012, **51**, 108–117; (c) S. Mandal, N. Paul, P. Banerjee, T. K. Mondal and S. Goswami, *Dalton Trans*., 2010, **39**, 2717–2726; (d) K.-W. Chan, Y.-K. Sau, Q.-F. Zhang, W.-Y. Wong, I. D. Williams and W.-H. Leung, *Eur. J. Inorg. Chem*., 2008, 4353–4359; (e) R. Y. C. Shin, V. W. L. Ng, L. L. Koh, G. K. Tan, L. Y. Goh and R. D. Webster, *Organometallics*, 2007, **26***,* 4555–4561; (f) E. P. L. Tay, S. L. Kuan, W. K. Leong and L. Y. Goh, *Inorg. Chem*., 2007, **46**, 1440–1450; (g) S. L. Kuan, E. P. L. Tay, W. K. Leong, L. Y. Goh, C. Y. Lin, P. M. W. Gill and R. D. Webster, *Organometallics*, 2006, **25**, 6134–6141.

(4) (a) M. Albrecht, *Chem. Rev*., 2010, **110**, 576–623; (b) M. C. Román-Martínez, J. A. Díaz-Auñón, C. Salinas-Martínez de Lecea and H. Alper, *Journal of Molecular Catalysis A: Chemical*., 2004, **213**, 177–182; (c) J. L. G. Fierroa, M. D. Merchán, S. Rojas and P. Terreros, *Journal of Molecular Catalysis A*: *Chemical*.,

2001, **166**, 255–264; (d) Y. Nishibayashi, M. Yamanashi, Y. Takagi and M. Hidai, *Chem. Commun*., 1997, 859–860.

(5) (a) J. Shearer, P. E. Callan, C. A. Masitas and C. A. Grapperhaus, *Inorg. Chem*., 2012, **51**, 6032−6045; (b) M. Hirotsu, C. Tsuboi, T. Nishioka and I. Kinoshita, *Dalton Trans*., 2011, **40**, 785–787; (c) K. Ouch, M. S. Mashuta and C. A. Grapperhaus, *Inorg. Chem*., 2011, **50**, 9904–9914.

(6) (a) S. D. Ornellas, T. E. Storr, T. J. Williams, C. G. Baumann and I. J. S. Fairlamb, *Curr. Org. Synth*., 2011, **8**, 79–101; (b) J. C. Love, L. A. Estroff, J. K. Kriebel, R. G. Nuzzo and G. M. Whitesides, *Chem. Rev*., 2005, **105**, 1103−1169.

(7) (a) M. A. Bowring, R. G. Bergman and T. D. Tilley, *J. Am. Chem. Soc*., 2013, **135**, 13121–13128; (b) T. S. Lobana, R. Sultana, R. J. Butcher, A. Castineiras, T. Akitsu, F. J. Fernandez and M. C. Vega, *Eur. J. Inorg. Chem*., 2013, 5161–5170; (c) Y. Jiao, J. Morris, W. W. Brennessel and W. D. Jones, *J. Am. Chem. Soc*., 2013, **135**, 16198–16212.

(8) (a) F. Guyon, M. Knorr, A. Garillon and C. Strohmann, *Eur. J. Inorg. Chem*., 2012, 282–291; (b) S. Kundu, W. W. Brennessel and W. D. Jones, *Organometallics*, 2011, **30**, 5147–5154; (c) N. Nakata, N. Furukawa, T. Toda and A. Ishii, *Angew. Chem., Int. Ed*., 2010, **49**, 5784–5787.

(9) K. Pramanik, U. Das, B. Adhikari, D. Chopra and H. Stoeckli-Evans, *Inorg. Chem*., 2008, **47**, 429–438.

(10) K. Izod, E. R. Clark, P. Foster, R. J. Percival, I. M. Riddlestone, W. Clegg and R. W. Harrington, *Chem. Eur. J*., 2013, **19**, 6094–6107.

(11) (a) J. S. Kim, J. H. Reibenspies and M. Y. Darensbourg, *J. Am. Chem. Soc*., 1996, **118**, 4115−4123; (b) M. Cha, S. C. Shoner and J. A. Kovacs, *Inorg. Chem*., 1993, **32**, 1860−1863.

(12) (a) C. A. Grapperhaus, K. B. Venna and M. S. Mashuta, *Inorg. Chem*., 2007, **46**, 8044–8050; (b) J. E. McDonough, J. J. Weir, K. Sukcharoenphon, C. D. Hoff, O. P. Kryatova, E. V. Rybak-Akimova, B. L. Scott, G. J. Kubas, A. Mendiratta, C. C. Cummins, *J. Am. Chem. Soc*., 2006, **128**, 10295–10303; (c) Y. Journaux, T. Glaser, G. Steinfeld, V. Lozana and B. Kersting, *Dalton Trans*., 2006, 1738–1748.

(13) (a) P. A. Stenson, A. Board, A. Marin-Becerra, A. J. Blake, E. S. Davies, C. Wilson, J. McMaster and M. Schröder, *Chem. Eur. J*., 2008, **14**, 2564–2576; (b) C.-Y. Chiang, J. Lee, C. Dalrymple, M. C. Sarahan, J. H. Reibenspies and M. Y. Darensbourg, *Inorg. Chem*., 2005, **44**, 9007–9016; (c) B. S. Chohan, S. C. Shoner, J. A. Kovacs and M. J. Maroney, *Inorg. Chem*., 2004, **43**, 7726–7734; (d) T. Osako, Y. Ueno, Y. Tachi and S. Itoh, *Inorg. Chem*., 2004, **43**, 6516–6518; (e) S. Kimura, E. Bill, E. Bothe, T. Weyhermüller, K. Wieghardt, *J. Am. Chem. Soc*., 2001, **123**, 6025–6039.

(14) (a) F. L. Benedito, T. Petrenko, E. Bill, T. Weyhermüller and K.Wieghardt, *Inorg. Chem*., 2009, **48**, 10913–10925; (b) S. Poturovic, M. S. Mashuta and C. A. Grapperhaus, *Angew. Chem., Int. Ed*., 2005, **44**, 1883–1887; (c) C. A. Grapperhaus, and S. Poturovic, *Inorg. Chem*., 2004, **43,** 3292–3298.

(15) (a) R. Chauhan, M. Moreno, D. M. Banda, F. P. Zamborini and C. A. Grapperhaus, *RSC Adv*., 2014, **4**, 46787–46790; (b) M. Hung and D. M. Stanbury, *Inorg. Chem*., 2005, **44**, 9952–9960.

(16) (a) C. A. Masitas M. S. Mashuta, and C. A. Grapperhaus, *Inorg. Chem*., 2010, **49**, 5344–5346; (b) R. A. Begum, A. A. Farah, H. N. Hunter and A. B. P. Lever, *Inorg. Chem*., 2009, **48**, 2018–2027; (c) T. Sriskandakumar, H. Petzold, P. C. A. Bruijnincx, A. Habtemariam, P. J. Sadler and P. Kennepohl, *J. Am. Chem. Soc*., 2009, **131**, 13355–13361; (d) D. Sellmann, K. Hein and F. W. Heineman, *Eur. J. Inorg. Chem*., 2004, 3136–3146; (e) C.-M. Lee, C.-H. Hsieh, A. Dutta, G.-H. Lee and W.-F. Liaw, *J. Am. Chem. Soc*., 2003, **125**, 11492–11493; (f) D. G. Ho, R. Ismail, N. Franco, R. Gao, E. P. Leverich, I. Tsyba, N. N. Ho, R. Bau and M. Selke, *Chem. Commun*., 2002, 570–571.

(17) (a) R. Y. C. Shin, G. K. Tan, L. L. Koh and L. Y. Goh, *Organometallics*, 2004, **23***,* 6293–6298; (b) T. Kondo and T. Mitsudo, *Chem. Rev*., 2000, **100**, 3205–3220; (c) T. B. Rauchfuss and D. M. Roundhill, *J. Am. Chem. Soc*., 1975, **97**, 3386–3392; (d) D. H. Busch, D. C. Jicha, M. C. Thompson, J. W. Wrathall and E. Blinn, *J. Am. Chem. Soc*., 1964, **86**, 3642–3650.

(18) (a) Y. Jiang, L. R. Widger, G. D. Kasper, M. A. Siegler and D. P. Goldberg, *J. Am. Chem. Soc*., 2010, **132**, 12214–12215; (b) A. Dey, S. P. Jeffrey, M. Y. Darensbourg, K. O. Hodgson, B. Hedman and E. I. Solomon, *Inorg. Chem*., 2007, **46**, 4989–4996; (c) T. M. Cocker and R. E. Bachman, *Chem. Commun.*, 1999, 875–876; (d) S. A. Mirza, M. A. Pressler, M. Kumar, R. O. Day and M. J. Maroney, *Inorg. Chem*., 1993, **32**, 977–987; (e) P. J. Farmer, T. Solouki, D. K. Mills, T. Soma, D. H. Russell, J. H. Reibenspies and M. Y. Darensbourg, *J. Am. Chem. Soc*., 1992, **114**, 4601–4605.

(19) (a) C. A. Masitas, M. Kumar, M. S. Mashuta, P. M. Kozlowski and C. A. Grapperhaus, *Inorg. Chem*., 2010, **49**, 10875–10881; (b) T. Arakawa, Y. Kawano, S. Kataoka, Y. Katayama, N. Kamiya, M. Yohda and M. Odaka, *J. Mol. Biol*., 2007, **366**, 1497–1509; (c) W. B. Tolman, *J. Biol. Inorg. Chem*., 2006, **11**, 261–271; (d) V. E. Kaasjager, E. Bouwman, S. Gorter, J. Reedijk, C. A. Grapperhaus, J. H. Reibenspies, J. J. Smee, M. Y. Darensbourg, A. Derecskei-Kovacs and L. M. Thomson, *Inorg. Chem*., 2002, **41**, 1837–1844; (e) J. C. Noveron, M. M. Olmstead and P. K. Mascharak, *J. Am. Chem. Soc*., 2001, **123**, 3247–3259.

(20) (a) D. Zhang, Y. Bin, L. Tallorin, F. Tse, B. Hernandez, E. V. Mathias, T. Stewart, R. Bau and M. Selke, *Inorg. Chem*., 2013, **52**, 1676–1678; (b) M. Tamura, K. Tsuge, A. Igashira-Kamiyamaa and T. Konno, *Chem. Commun.*, 2011, **47**, 12464–12466; (c) R. Acharyya, S. Dutta, F. Basuli, S.-M. Peng, G.-H. Lee, L. R. Falvello, S. Bhattacharya, *Inorg. Chem*., 2006, **45**, 1252–1259; (d) C. A. Grapperhaus, S. Poturovic and M. S. Mashuta, *Inorg. Chem*., 2005, **44**, 8185–8187; (e) P. Römbke, A. Schier and H. Schmidbaur, *Dalton Trans*., 2001, 2482–2486; (f) C. A. Grapperhaus, M. J. Maguire, T. Tuntulani and M. Y. Darensbourg, *Inorg. Chem*., 1997, **36***,* 1860–1866.

(21) (a) J. Pratihar, D. Patra and S. Chattopadhyay, *J. Organomet. Chem*., 2005, **690**, 4816–4821; (b) M. Lersch and M. Tilset, *Chem. Rev*., 2005, **105**, 2471–2526; (c) J. Dupont, C. S. Consorti and J. Spencer, *Chem. Rev*., 2005, **105**, 2527–2571.

(22) (a) C. Elsässer, N. Takeuchi, K. M. Ho, C. T. Chan, P. Braun and M. Fähnle, *Phys.: Condens. Matter*., 1990, **2**, 4371–4394; (b) P. Pyykko, *Chem. Rev*., 1988, **88**, 563–594.

(23) C. A. Grapperhaus, C. S. Mullins, P. M. Kozlowski and M. S. Mashuta, *Inorg. Chem*., 2004, **43**, 2859–2866.

(24) (a) L. Dong, S. B. Duckett, K. F. Ohman and W. D. Jones, *J. Am. Chem. Soc*., 1992, **114**, 151–160; (b) W. D. Jones and L. Dong, *J. Am. Chem. Soc*., 1991, **113**, 559–564.

(25) Formation of R^+ by heterolytic bond breaking is not a realistic mechanism for the C–S bond rupture since the formation of any R–R is rather unexpected *via* alkyl cations. Moreover, formation of the corresponding alkane *via* hydride abstraction appears to be less likely. The other options include (1) two electron reductive cleavage and the formation of R^- which proceeds through an intermediate of the Ir(I) fragment $[Ir(L^{SR})(PPh_3)]$ and (2) an initial formal reduction at the metal center to the metastable intermediate $[Ir^{II}(L^{SR})Cl(PPh_3)]$ followed by single-electron transfer (SET) to the σ^* orbital of S–C(alkyl) bond with subsequent release of $R^\bullet$ as cleavage product.

(26) The plausible radical reactions can be written as:

$PhCH_2^\bullet + EtOH \rightarrow PhCH_3 + EtO^\bullet$

$PhCH_2^\bullet + EtO^\bullet \rightarrow PhCH_2OEt$

$PhCH_2^\bullet + [Cl–Ir^{III}] \rightarrow PhCH_2Cl + [Ir^{II}]$

$2PhCH_2^\bullet \rightarrow PhCH_2CH_2Ph$

(27) J. M. O'Connor, K. D. Bunker, A. L. Rheingold and L. Zakharov, *J. Am. Chem. Soc*., 2005, **127**, 4180–4181.

(28) A. K. Mahapatra, S. Dutta, S. Goswami, M. Mukherjee, A. K. Mukherjee and A. Chakravorty, *Inorg. Chem*., 1986, **25**, 1715–1721.

(29) K. Pramanik, M. Shivakumar, P. Ghosh and A. Chakravorty, *Inorg. Chem*., 2000, **39**, 195–199.

(30) M. Montalti, A. Credi, L. Prodi and M. T. Gandolfi, *Handbook of Photochemistry*, CRC Press, Boca Ration, FL, 2006.

(31) (a) S. Roy, S. Pramanik, T. Ghorui and K. Pramanik, *RSC Adv*., 2015, **5**, 22544–22559; (b) S. Pramanik, S. Roy, T. Ghorui, S. Ganguly and K. Pramanik, *Dalton Trans*., 2014, **43**, 5317–5334; (c) R. Tanaka, P. Viehmann and S. Hecht, *Organometallics*, 2012, **31**, 4216–4220; (d) E. Marchi, M. Baroncini, G. Bergamini, J. V. Heyst, F. Vögtle and P. Ceroni, *J. Am. Chem. Soc*., 2012, **134**, 15277−15280; (e) A. S. Roy, P. Saha, N. D. Adhikary and P. Ghosh, *Inorg. Chem*., 2011, **50**, 2488–2500; (f) K. Pramanik and B. Adhikari, *Polyhedron*, 2010, **29**, 1015−1022; (g) H. Nishihara, *Chem. Rev*., 2005, **249**, 1468–1475.

(32) (a) S. E. Livingstone, *J. Chem. Soc*., 1956, 437–440; (b) A. Burawoy and C. E. Vellins, *J. Chem. Soc*., 1954, 90–95; (c) R. L. Shriner, H. C. Struck and W. J. Jorison, *J. Am. Chem. Soc*., 1930, **52**, 2060–2069.

(33) R. Acharyya, F. Basuli, R.-Z. Wang, T. C. W. Mak and S. Bhattacharya, *Inorg. Chem*., 2004, **43**, 704−711.

Graphic for Manuscript

Iridium-Mediated C–S Bond Activation and Transformations: Organoiridium(III) Thioether, Thiolato, Sulfinato and Thiyl Radical Compounds. Synthesis, Mechanistic, Spectral, Electrochemical and Theoretical Aspects

Iridium-Mediated C–S bond scission by uncommon SET reductive process: Exploration of S-centered reactivity of organoiridium(III) thiolato through the derivatization along with generation of thiyl radical.